

ENSO teleconnections with Australian rainfall in coupled model simulations of the last millennium

Josephine R. Brown¹ · Pandora Hope¹ · Joelle Gergis^{2,3} · Benjamin J. Henley²

Received: 8 March 2015 / Accepted: 25 August 2015 / Published online: 5 September 2015
© Springer-Verlag Berlin Heidelberg 2015

Abstract El Niño–Southern Oscillation is the major source of interannual rainfall variability in the Australian region, with the strongest influence over eastern Australia. The strength of this regional ENSO–rainfall teleconnection varies in the observational record. Climate model simulations of the “last millennium” (850–1850 C.E.) can be used to quantify the natural variability of the relationship between ENSO and Australian rainfall on decadal and longer time scales, providing a baseline for evaluating future projections. In this study, historical and last millennium (LM) simulations from six models were obtained from the Coupled Model Intercomparison Project Phase 5 and Palaeoclimate Modelling Intercomparison Project Phase 3. All models reproduce the observed negative correlation between September to February (SONDJF) eastern Australian rainfall and the NINO3.4 index, with varying skill. In the LM simulations, all models produce decadal-scale cooling over eastern Australia in response to volcanic forcing, as well as a long-term cooling trend. Rainfall variability over the same region is not strongly driven by external forcing, with each model simulating rainfall anomalies of different phase and magnitude. SONDJF eastern

Australian rainfall is strongly correlated with ENSO in the LM simulations for all models, although some models simulate periods when the teleconnection weakens substantially for several decades. Changes in ENSO variance play a role in modulating the teleconnection strength, but are not the only factor. The long-term average spatial pattern of the ENSO–Australian rainfall teleconnection is similar in the LM and historical simulations, although the spatial pattern varies over time in the LM simulations.

Keywords El Niño–Southern Oscillation · Last millennium · Coupled climate model · Rainfall variability · Australia

1 Introduction

Australian rainfall is highly variable on a range of time-scales (e.g. Nicholls et al. 1997), with instrumental records documenting multi-year droughts and extended periods of flooding. The surrounding oceans strongly influence rainfall across the Australian continent, and consequently droughts and floods are broadly spatially coherent (e.g. Wang and Hendon 2007; Risbey et al. 2009). This is particularly true for eastern Australia, a region that contains the majority of the Australian population and the major agricultural region of the Murray–Darling Basin (e.g. Gallant et al. 2012). Communities and ecosystems have adapted to the frequency and magnitude of present day rainfall variability, and may be highly sensitive to any future changes. It is therefore of interest to understand the longer term variability of eastern Australian rainfall and its relationship with ENSO, to provide a baseline for comparison with future climate projections.

Electronic supplementary material The online version of this article (doi:10.1007/s00382-015-2824-6) contains supplementary material, which is available to authorized users.

✉ Josephine R. Brown
j.brown@bom.gov.au

¹ Bureau of Meteorology, 700 Collins St, Melbourne, VIC 3000, Australia

² School of Earth Sciences, University of Melbourne, Parkville, VIC 3010, Australia

³ ARC Centre of Excellence for Climate System Science, University of Melbourne, Parkville, VIC 3010, Australia

Climate model simulations of the last millennium, the period 850 to 1850 C.E. (Common Era, omitted hereafter), were carried out as part of the Coupled Modelling Intercomparison Project Phase 5 (CMIP5, Taylor et al. 2012) and Palaeoclimate Modelling Intercomparison Project Phase 3 (PMIP3, Braconnot et al. 2012). Model inputs include the effects of volcanic aerosols, solar variability and greenhouse gas changes (Schmidt et al. 2012). While these forcings are relatively weak on multi-decadal and longer timescales compared with other periods such as the Last Glacial Maximum or future enhanced greenhouse gas scenarios (Schmidt et al. 2014), the last millennium provides an opportunity to examine natural (both forced and internal) variability over a sufficiently long period to characterise multi-year, decadal and longer variations in rainfall. The last millennium is also the period containing the most accurately dated palaeoclimate records (e.g. tree rings and coral records) that can be directly calibrated against instrumental climate records (Neukom and Gergis 2012).

The major influence on present day rainfall variability across eastern Australia is the El Niño–Southern Oscillation (ENSO), while other drivers of rainfall variability in this region include the Indian Ocean Dipole, Southern Annular Mode and atmospheric blocking (e.g. Risbey et al. 2009). The canonical association, or “teleconnection”, between ENSO and Australian rainfall includes a strong negative relationship between rainfall in eastern Australia and sea surface temperatures in the central equatorial Pacific. Thus, dry conditions are typically associated with El Niño events and wet conditions with La Niña events (e.g. Ropelewski and Halpert 1987; Power et al. 1998; Diaz et al. 2001; Risbey et al. 2009). During El Niño events, warmer waters are displaced from the western Pacific to the central and eastern Pacific, and convective activity and rainfall are also displaced eastward away from Australia. The South Pacific Convergence Zone shifts north and east during El Niño, and south and west during La Niña events (e.g. Vincent et al. 2011), which influences rainfall over the southeast Queensland region in particular (Cai and van Rensch 2012).

The teleconnection between ENSO and Australian rainfall is known to vary through time in the instrumental period (e.g. Nicholls et al. 1997; Kestin et al. 1998; Gallant et al. 2013; Ashcroft et al. 2014). Observed variability of the ENSO–Australian rainfall relationship is associated with the Inter-decadal Pacific Oscillation (IPO, Power et al. 1998; Arblaster et al. 2002; Power et al. 2006), with the positive phase of the IPO being associated with a weakened relationship between ENSO and Australian rainfall. In addition, palaeoclimate reconstructions suggest that the longer term relationship between ENSO and Australian rainfall is non-stationary (e.g. Hendy et al. 2003; Gergis et al. 2012). This study makes use of the CMIP5–PMIP3 suite of last

millennium coupled model simulations to explore the variability of Australian rainfall over 1000 years. Historical and last millennium simulations are used to assess the hypothesis that ENSO–eastern Australian rainfall teleconnections have remained stable on multi-century time scales. We compare previous studies with results from the CMIP5–PMIP3 coupled models, examining both the temporal and spatial stationarity of the ENSO–rainfall teleconnection.

The structure of the paper is as follows. In Sect. 2, the Data and Methods are described. In Sect. 3, the ability of the models to simulate present day ENSO–rainfall relationships is evaluated. In Sect. 4, ENSO–eastern Australian rainfall teleconnections are examined in the last millennium simulations. Finally, Discussion and Conclusions are given in Sect. 5.

2 Data and methods

2.1 Data and models

The results from six coupled climate models that carried out simulations of both the historical period (“HIST”, 1850–2000 or later) and last millennium (“LM”, 850–1850) were analysed. The models are: BCC-CSM1.1, CCSM4, CSIRO-Mk3L-1-2, GISS-E2-R, IPSL-CM5A-LR, and MPI-ESM-P (see Table 5.A.1 in Appendix of Masson-Delmotte et al. 2013 for further information and references). All model output was converted to a $1.5^\circ \times 1.5^\circ$ grid prior to further processing.

Model rainfall and temperature output was compared with observational climate data over the instrumental period. The Australian Water Availability Project (AWAP) rainfall data set (Jones et al. 2009) at 0.25° resolution was used to calculate average rainfall over eastern Australia, defined here as the land areas bounded by 10°S – 45°S , 140°E – 155°E . For spatial information over the broader Pacific domain, the Global Precipitation Climatology Project (GPCP) Version 2 global gridded rainfall data set (Adler et al. 2003) was used. NINO3.4 region (5°S – 5°N , 170°W – 120°W) sea surface temperature (SST) values were calculated using the Extended Reconstructed Sea Surface Temperature (ERSST) data set (Smith and Reynolds 2004).

2.2 Methods

For the historical (HIST) simulations, results were analysed for the years 1900–2000, which is the common period of overlap between the model simulations and instrumental Australian climate data (a shorter period is used for global observed rainfall data, which is available from 1979 onwards). For the last millennium (LM) simulations, all years (850–1850) are used unless otherwise

stated. Seasonal averages are calculated over the austral Spring and Summer months of September to February (SONDJF), as this is when ENSO conditions are generally at their peak maturity (e.g. Rasmusson and Carpenter 1982) and there is a strong correlation between eastern Australian rainfall and ENSO (e.g. Power et al. 1998). While the strongest observed correlations are between September to November rainfall and December to February ENSO indices, the longer SONDJF averaging period is used in this study to allow for some variation in timing of the peak ENSO–eastern Australian rainfall teleconnection in the models.

Running correlations and variances were calculated using a 30-year sliding window for both HIST and LM simulations. Where running correlations and variance are plotted, the values are plotted against the central year (15th year of 30-year window). Where stated, data were detrended by removing the least squares linear trend in order to focus on interannual to decadal variability. The statistical significance of correlations was calculated by first reducing the degrees of freedom of the data to account for auto-correlation (Bretherton et al. 1999).

3 Eastern Australian rainfall and ENSO in historical simulations

3.1 Rainfall variability

The SONDJF average rainfall was calculated over eastern Australia (land grid points in the domain 10°S–45°S, 140°E–155°E) for the observed AWAP data set and the six climate models over the period 1900–2000, shown in Fig. 1. The observed rainfall (Fig. 1g) varies considerably from year to year and on multi-decadal time scales. For example, particularly wet conditions occurred during La Niña events, including the 1916–1918 and the 1970–1972 and 1973–1976 events, while particularly dry conditions are evident at the beginning of the record (the “Federation” Drought of 1895–1902) and in the early 1980s associated with the strong El Niño of 1982–1983. The model HIST simulations (Fig. 1a–f) also capture considerable interannual and decadal variability of rainfall, with varying magnitudes, although all models have weaker variability than the observations. The standard deviation of model rainfall variability (see Fig. 1; Table 1) varies by a factor of two, from the relatively weak variability of IPSL-CM5A-LR and GISS-E2-R to the stronger variability of BCC-CSM1.1 and CCSM4, which are closest to the observed variability. Note that there are differences in the sign and duration of rainfall anomalies simulated by each model, reflecting the role of internal climate variability, including ENSO, in driving these anomalies.

3.2 ENSO–rainfall teleconnections

As discussed in Sect. 1, a major driver of interannual rainfall variability over eastern Australia is ENSO. Before examining the long-term relationship between Australian rainfall and ENSO in palaeoclimate simulations of the last 1000 years, we examine the ability of the models to capture the observed relationship over the 1900–2000 instrumental period. First we consider the spatial pattern of the ENSO–eastern Australian rainfall relationship (Fig. 2) and then evaluate the nonlinear nature of the relationship (Fig. 3). Finally, we consider how the relationship varies in time over the instrumental period (Fig. 4).

The observed spatial correlation between ENSO and rainfall was calculated from the NINO3.4 SST and GPCP gridded rainfall data averaged over SONDJF for the years 1979–2008 (Fig. 2g). The observed teleconnection pattern is compared with the pattern simulated by the six coupled climate models over the period 1900–2000 (Fig. 2a–f). The observed correlation pattern includes negative anomalies in the region of the Indonesian and Australian monsoon, and a band of anomalies stretching to the southwest, corresponding to the movement of the SPCZ in response to ENSO. The models broadly reproduce this pattern, although the SPCZ anomaly tends to be too zonal, as in many CMIP5 models (Brown et al. 2013), and the models tend to simulate the boundary between negative and positive anomalies in the equatorial western Pacific too far to the west, also a common coupled model bias (e.g. Grose et al. 2014). Over eastern Australia, all models capture the negative correlation between the NINO3.4 index and rainfall, although the magnitude and spatial pattern of the correlations varies considerably. The match between the observed and simulated spatial pattern of rainfall response to ENSO is quantified using the pattern correlations over the domain 15°N–50°S, 100°E–160°W (see Table 1). The models with the highest pattern correlation are BCC-CSM1.1, CCSM4 and GISS-E2-R, while IPSL-CM5A-LR has the lowest pattern correlation, due to incorrect negative correlations over Tasmania and to the north of Australia over New Guinea.

The temporal correlation between SONDJF eastern Australian rainfall and NINO3.4 indices was also calculated (see Table 1). The observed correlation between eastern Australian rainfall and NINO3.4 is -0.55 for the years 1900–2000. Although all models simulate a weaker correlation than observations, the model correlations are close to the observed relationship, with the exception of CSIRO-Mk3L, which has a correlation of less than half this strength ($r = -0.22$).

The non-linear nature of the relationship between ENSO and Australian rainfall has been identified in instrumental records (e.g. Power et al. 1999). Typically, La Niña events lead to larger positive rainfall anomalies than the

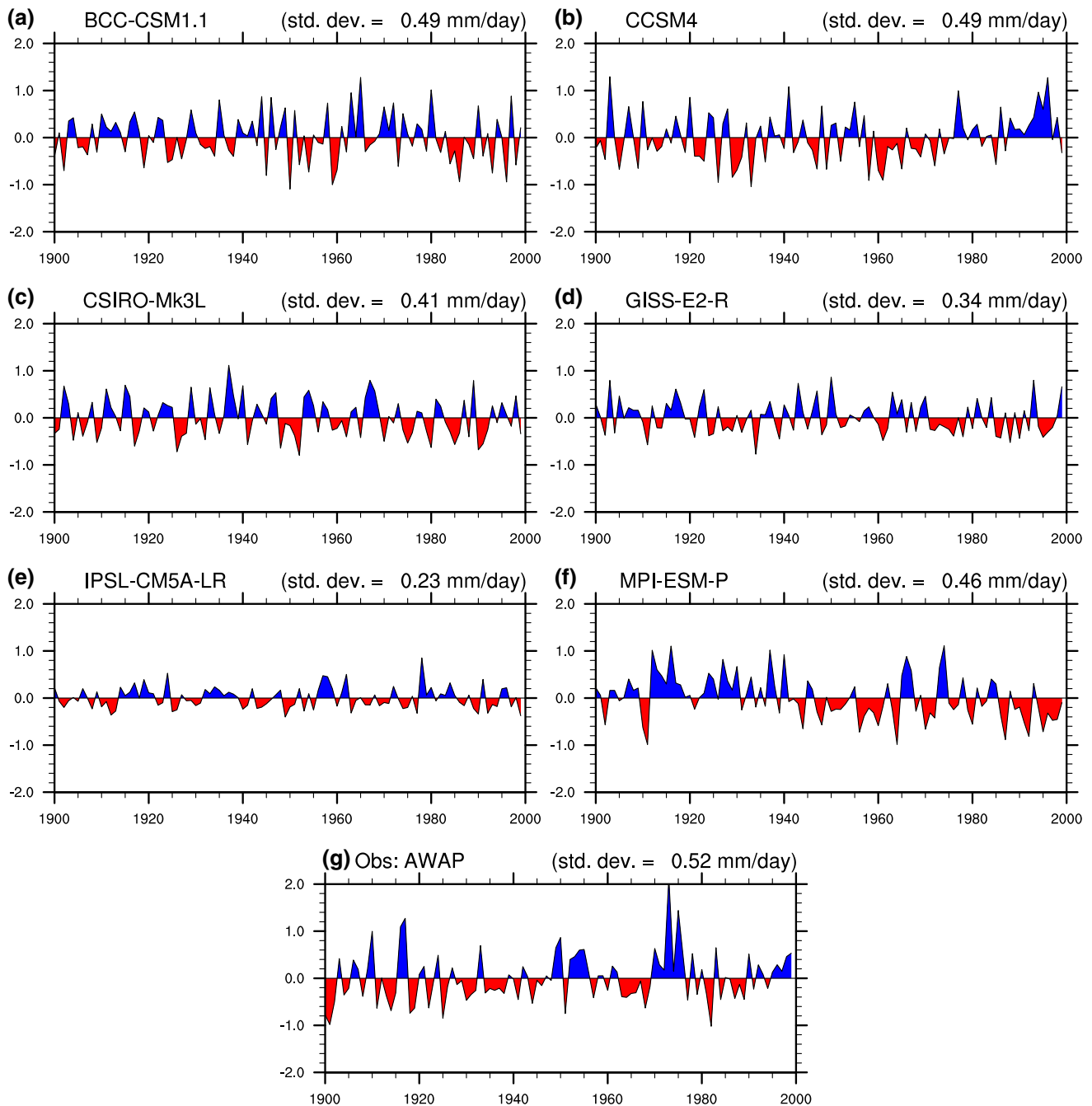


Fig. 1 September to February average eastern Australian rainfall anomalies (mm/day) for 1900–2000 for models **a** BCC-CSM1.1, **b** CCSM4, **c** CSIRO-Mk3L, **d** GISS-E2-R, **e** IPSL-CM5A-LR,

and **f** MPI-ESM-P, and **g** AWAP observations. Rainfall is averaged over land only in the eastern Australian domain (10°S–45°S, 140°E–155°E). The standard deviation of rainfall is given at *top right*

corresponding negative rainfall anomalies associated with El Niño events. This relationship is seen in observations (Fig. 3g), with the slope of the regression between SONDJF NINO3.4 and eastern Australian rainfall being twice as steep for years with NINO3.4 < 0 (“La Niña years”) than years with NINO3.4 > 0 (“El Niño years”). Three of the six models are able to reproduce this nonlinearity: CCSM4, CSIRO-Mk3L and GISS-E2-R, based on having a NINO3.4-rainfall slope that is more than 50 %

larger for La Niña years than for El Niño years (Fig. 3b–d). BCC-CSM1.1 and MPI-ESM-P incorrectly have larger rainfall anomalies during El Niño events.

The temporal stability of the observed and modelled ENSO–eastern Australian rainfall teleconnection in the historical period was examined using 30-year running correlations of SONDJF rainfall and NINO3.4 (Fig. 4). The figure also shows the 30-year running variance of NINO3.4 for the same period. In the instrumental record (Fig. 4g),

Table 1 Observed and model variability of eastern Australian (EA) rainfall and ENSO: rainfall standard deviation, NINO3.4 standard deviation, temporal correlation between EA rainfall and NINO3.4 and pattern correlation between observed and simulated rainfall response to ENSO (i.e. grid point correlation of rainfall and NINO3.4)

Name	EA rainfall SD (mm/day)	NINO3.4 SD (°C)	Temporal correlation: EA rainfall and NINO3.4	Pattern correlation: ENSO rainfall response
Observations*	0.52	0.92	-0.55	-
BCC-CSM1-1	0.49	0.77	-0.41	0.78
CCSM4	0.49	1.23	-0.46	0.75
CSIRO-Mk3-L	0.41	0.63	-0.22	0.69
GISS-E2-R	0.34	0.67	-0.37	0.74
IPSL-CM5A-LR	0.23	0.69	-0.49	0.39
MPI-ESM-P	0.46	0.82	-0.50	0.54

All data are SONDJF averages. All temporal and pattern correlations are significant at the 5 % level

* Note that the observed NINO3.4-rainfall correlation pattern is calculated using GPCP rainfall for the period 1979–2008, while all other observed rainfall is AWAP data for period 1900–2000

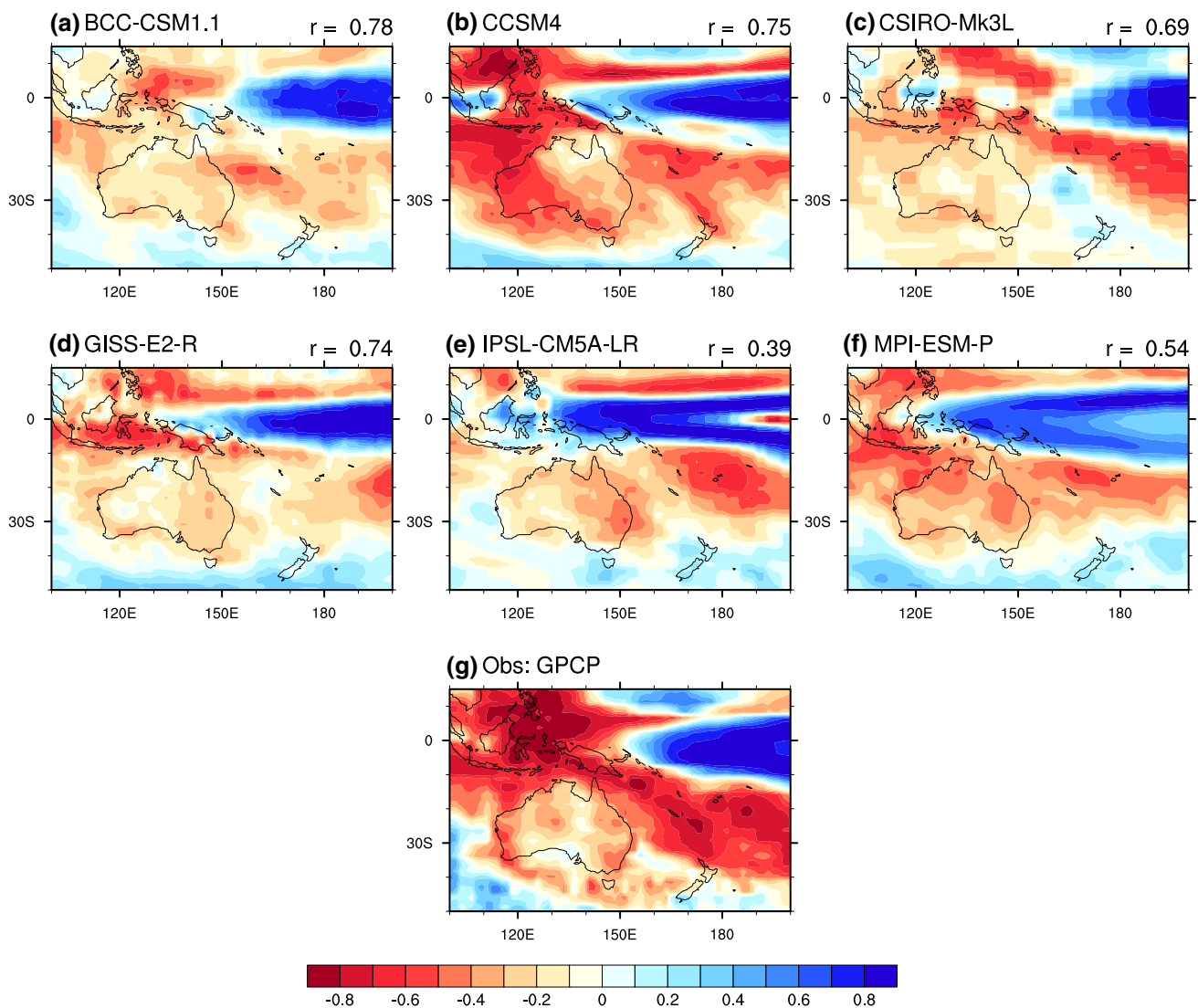


Fig. 2 Correlation between September to February rainfall and NINO3.4 index for models (a–f) and g GPCP observations. Note that model correlations were calculated for period 1900–2000, and observed correlations were calculated for 1979–2008. All time series

were linearly detrended before correlations were calculated. The spatial pattern correlation coefficient between each model and the observed correlation patterns over the domain shown (15°N–50°S, 100°E–160°W) is given at *top right*

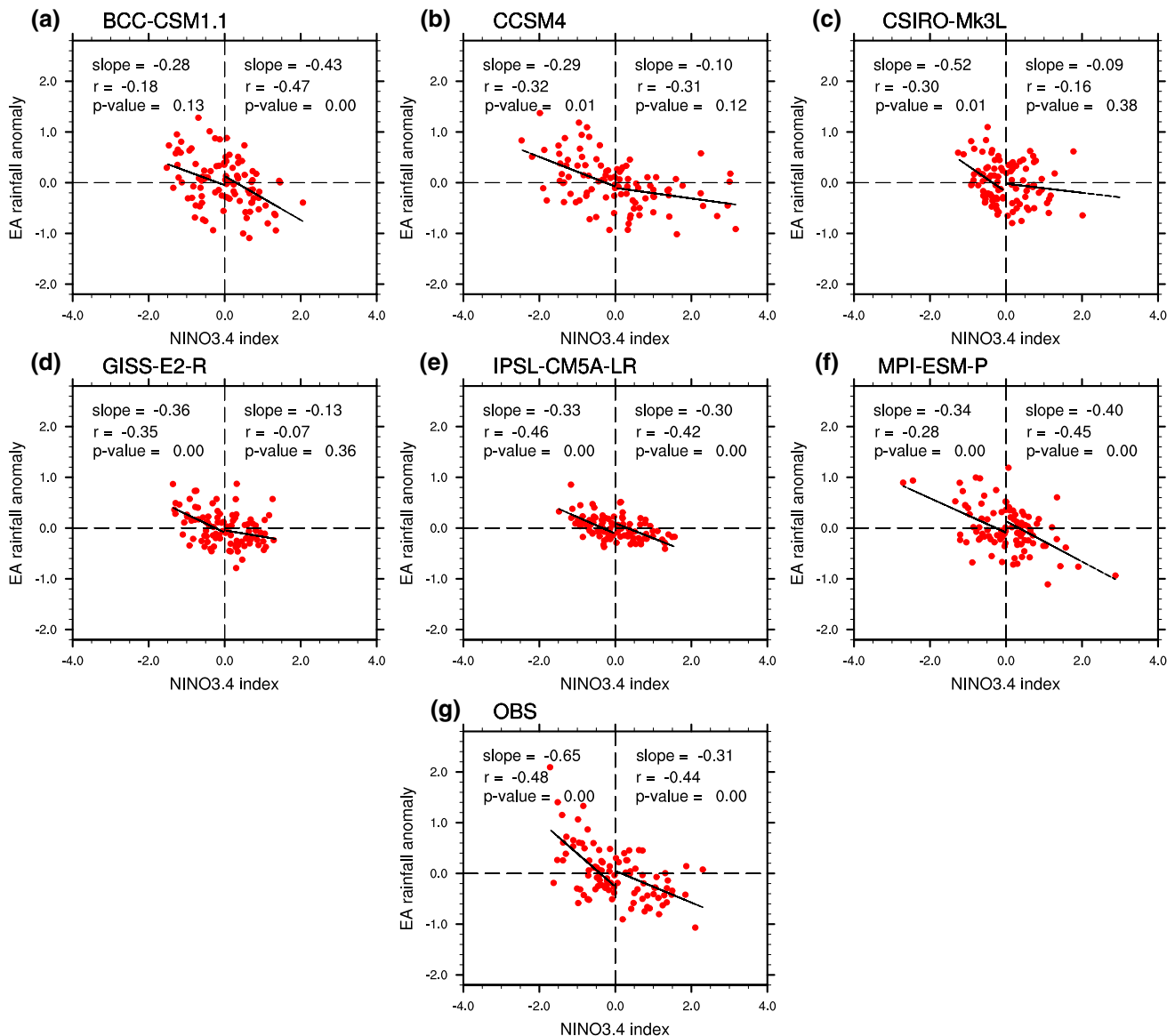


Fig. 3 Model (a–f) and observed g September to February eastern Australian rainfall (mm/day) versus NINO3.4 index ($^{\circ}\text{C}$) for 1900–2000. All data are linearly detrended. Lines of best fit are calculate

for all points with NINO3.4 > 0 and NINO3.4 < 0. The slopes of the regression lines, Spearman rank correlation coefficients and p values are also shown

there is a period of reduced strength of correlations centred around 1940. This reduced ENSO–eastern Australian rainfall correlation corresponds to a period of weaker ENSO variance and fewer ENSO events, as identified in previous studies (e.g. Kestin et al. 1998).

The models simulate substantial variations in the strength of the ENSO–rainfall correlation, including a weakening trend (CCSM4), a strengthening trend (GISS-E2-R, IPSL-CM5A-LR) and periods of teleconnection breakdown similar to or greater than the weakening observed in the 1940s (CSIRO-Mk3L and MPI-ESM-P). Trends are significant at the 5 % confidence level. In

observations and all models except CCSM4, teleconnection strength is significantly inversely correlated with ENSO variance. The relationship between teleconnection strength and ENSO variance is stronger for IPSL-CM5A-LR and MPI-ESM-P than for observations.

3.3 Summary of model performance

The ability of the six CMIP5–PMIP3 models to simulate the variability of eastern Australian rainfall and the teleconnection with ENSO for the historical period is summarised in Table 1. While some models appear to have ENSO

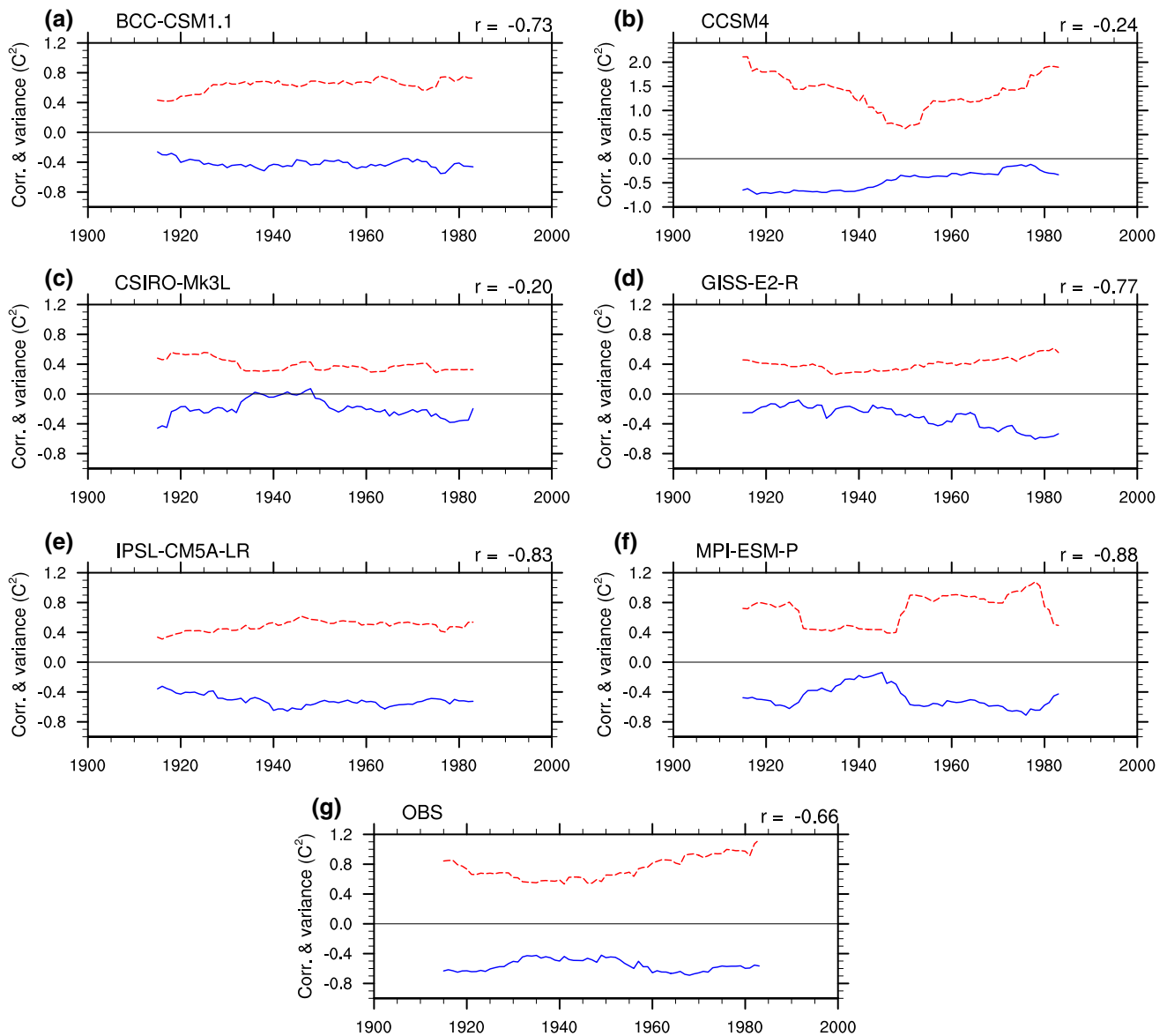


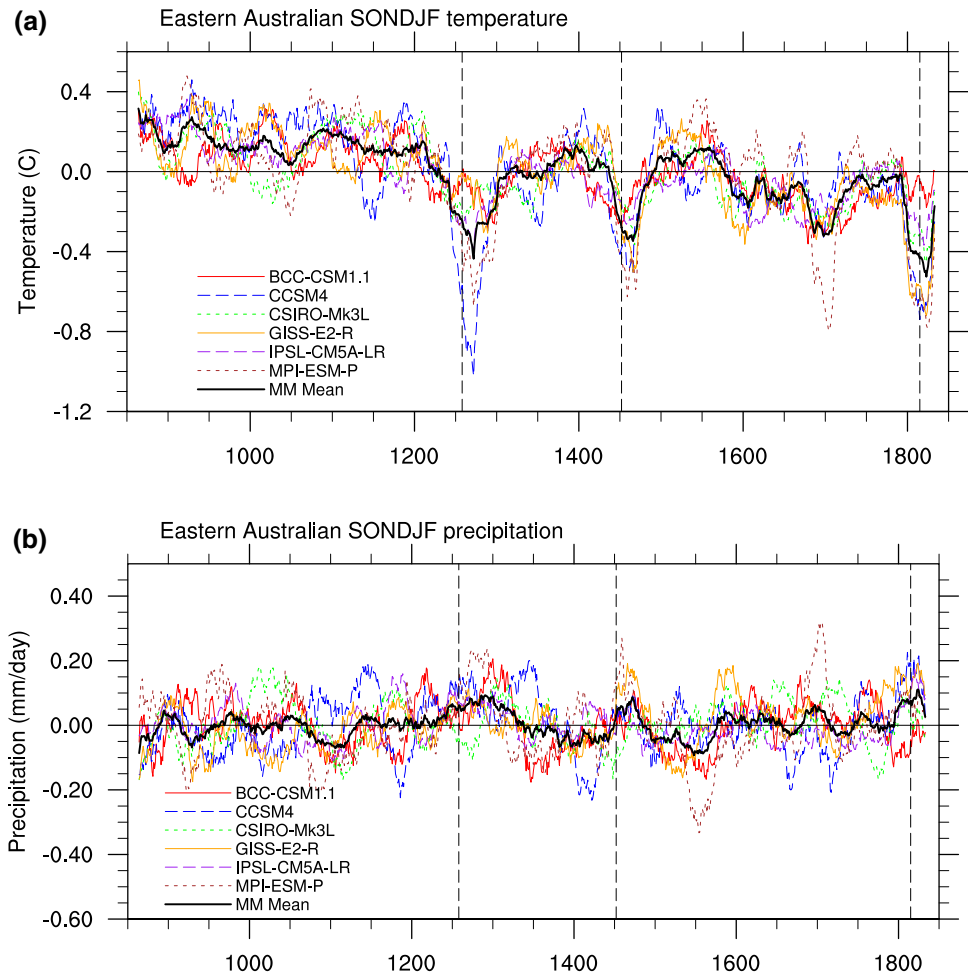
Fig. 4 30-year running correlations of September to February eastern Australian rainfall and NINO3.4 index for 1900–2000 (blue solid line) and 30-year running variance ($^{\circ}\text{C}^2$) of SONDJF NINO3.4 index (red dashed line) for models (a–f) and AWAP observations (g). All

time series were linearly detrended before calculating running correlations. Correlations between the two time series are given at the top right. Note (b) has different y-axis scale

characteristics that more closely match observations, it is important to note that the observational record may be insufficient to capture the full range of ENSO behaviour (e.g. Wittenberg 2009). We therefore use all six models to investigate the climate of the last millennium. However, as the focus of this study is eastern Australian rainfall variability, we have limited confidence in IPSL-CM5A-LR due to its low rainfall variability and poor simulation of the regional rainfall response to ENSO. CSIRO-Mk3L has a particularly low correlation between eastern Australian rainfall and ENSO, but is able to simulate other aspects of ENSO and regional rainfall variability reasonably well.

We also note that King et al. (2014) evaluated the ability of CMIP5 models to simulate the ENSO–eastern Australian rainfall relationship, and found that BCC-CSM1-1 and GISS-E2-R failed to capture aspects of the asymmetric or nonlinear relationship. An evaluation of the ENSO–rainfall relationship over the south-east Australian region also found that these two models (as well as other CMIP5 models not included in this study) did not capture the observed rainfall variability (Lewis and Karoly 2015), whereas CCSM4, MPI-ESM-P and IPSL-CM5A-LR were able to simulate the relationship. CSIRO-Mk3L was not included in the studies of King et al. (2014) or Lewis and Karoly (2015).

Fig. 5 30-year running average eastern Australian SONDJF anomalies of **a** temperature (°C) and **b** precipitation (mm/day) for LM simulations (850–1850). The multi-model (MM) mean is also shown (*thick black line*). Data is averaged over land only in the eastern Australian domain (10°S–45°S, 140°E–155°E). The dates of major volcanic eruptions at 1258, 1452 and 1815 are shown as *vertical dashed lines* for reference



4 Rainfall variability in last millennium simulations

4.1 Variability of eastern Australian climate

To assess the possible role of external forcing of ENSO–rainfall teleconnections, the SONDJF average surface temperature and rainfall over eastern Australia were calculated for each year of the LM simulations. The 30-year running average values are shown in Fig. 5 for all six CMIP5–PMIP3 models as well as the multi-model mean value. The temperature time series (Fig. 5a) show some common features for all models, including cooling events associated with major volcanic eruptions around 1258, 1452 and 1815 (see Landrum et al. 2013), while some events are only simulated by one model, e.g. MPI-ESM-P has a large regional cooling event around 1700. There is also a modest cooling trend over the entire LM simulation which is shared by all models (0.3–0.5 °C per 1000 years, significant at the 5 % level in all cases), consistent with the larger scale Southern Hemisphere trend in LM simulations (e.g. Fernández-Donado et al. 2013; Landrum et al. 2013). A similar long-term cooling trend

is found in regional temperature reconstructions of the past one to two millennia, thought to be associated with changes in solar irradiance, volcanic activity, land use and orbitally-driven insolation (PAGES 2k Consortium 2013).

In contrast with temperature, there is less coherent variability between models in the eastern Australian SONDJF rainfall record in the LM simulations (Fig. 5b). There are multi-decadal rainfall increases during the cooler periods following the largest volcanic eruptions in the majority of models. The increases result in significant positive anomalies in the multi-model mean following the major volcanic eruptions around 1258, 1452 and 1815 (the 10-year mean following each eruption is above the 95th percentile of values calculated from sampling running 10-year blocks of the record). There is no long-term trend in regional rainfall evident over the LM simulations. Apart from the volcanic signals, each model simulates rainfall variability on multi-decadal timescales that is out of phase with other models, with correlations between models that are not significant at the 5 % confidence level once autocorrelation is taken into account. This implies that most of the simulated rainfall variability in this region is due to the internal dynamics of

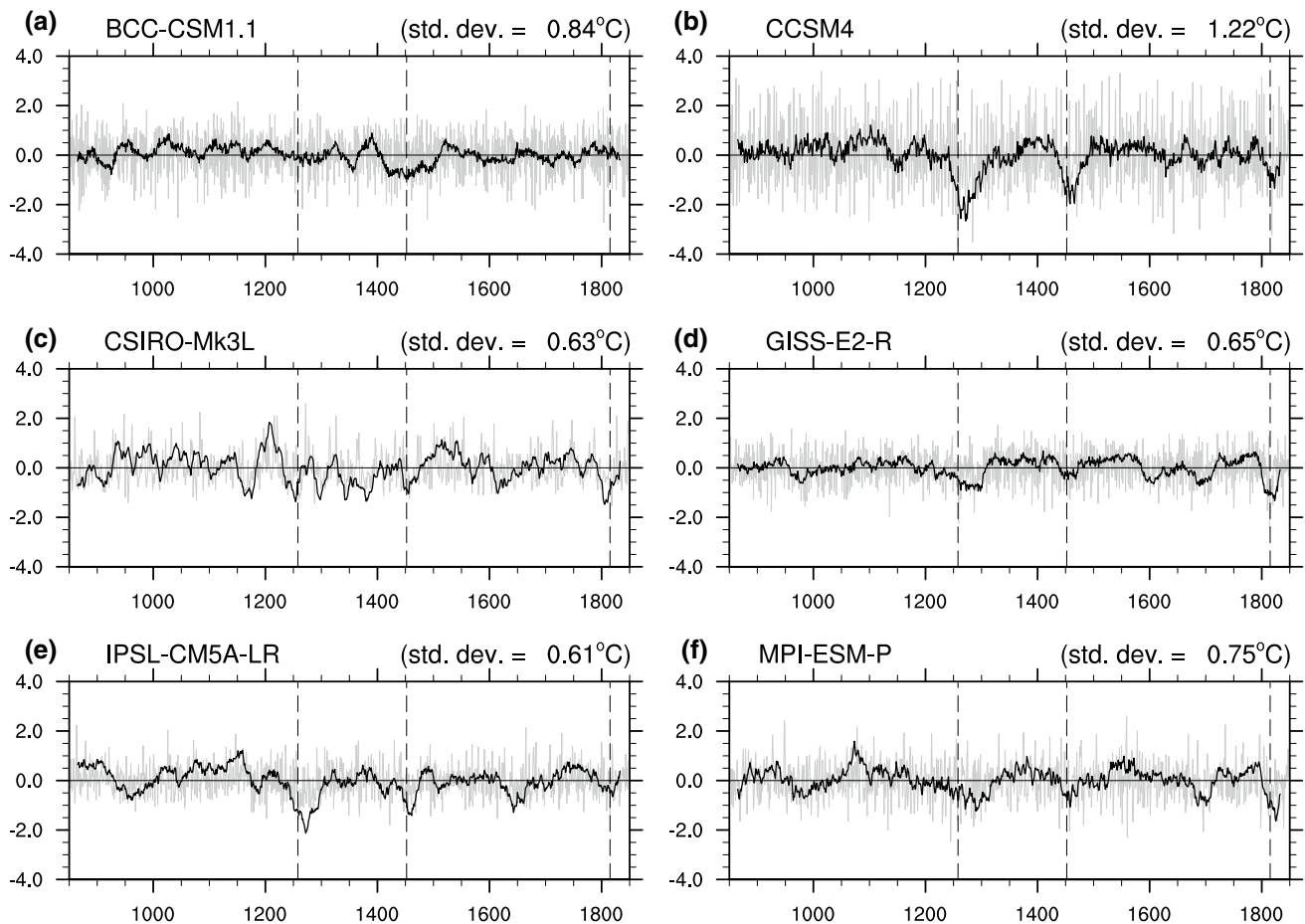


Fig. 6 Annual SONDJF NINO3.4 index ($^{\circ}\text{C}$) and 30-year running average (multiplied by 4 for visual comparison) for LM simulations. All time series are linearly detrended. The dates of major volcanic eruptions at 1258, 1452 and 1815 are shown as *vertical dashed lines* for reference

the climate system, which includes ENSO as well as other modes of variability.

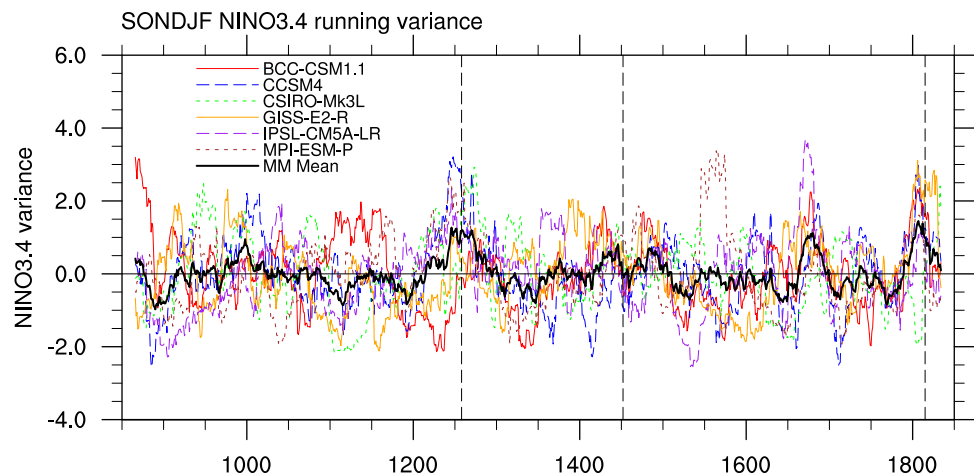
4.2 Variability of ENSO

Next, we consider the temporal variability of ENSO in the LM model simulations. Changes in ENSO period and other spectral characteristics are the subject of a companion study (Hope, P., B.J. Henley, J. Gergis, J. R. Brown and H. Ye, *Time-varying spectral characteristics of ENSO indices over the last millennium—in preparation*). The SONDJF NINO3.4 index was calculated for each model for all years from 850 to 1850, with both the annual values and 30-year running mean values shown in Fig. 6. The models all simulate variability of NINO3.4 SSTs on interannual and multi-decadal timescales. In particular, all of the models simulate significant cool NINO3.4 SST anomalies following one or more of the major volcanic eruptions. (Significance is estimated here as for the rainfall anomalies in Fig. 5, i.e. the 10-year mean following each eruption is below the 5th percentile of values calculated from sampling running 10-year

blocks of the record). While this cooling may represent tropics-wide SST cooling rather than an ENSO-like SST anomaly, comparison with a modified Southern Oscillation Index (calculated using eastern and western equatorial Pacific boxes following the approach of Power and Kociuba 2011, see Supplementary Figure 1) indicates that these periods were also characterised by La Niña-like changes in the large-scale sea level pressure field. Previous studies have found that volcanic events modify the likelihood of ENSO events in the following years, although the precise timing and mechanisms remain the subject of debate (e.g. Adams et al. 2003; Mann et al. 2005; Emile-Geay et al. 2008; McGregor and Timmermann 2011). Ault et al. (2013) identified volcanic forcing as the major source of low-frequency variability in NINO3.4 SSTs in the CMIP5–PMIP3 model last millennium simulations.

To identify changes in the amplitude of ENSO, the running variance of the SONDJF NINO3.4 index was calculated in a 30-year sliding window for each of the LM simulations, shown as the normalised anomaly (variance is divided by its standard deviation for each model) for easier

Fig. 7 SONDJF NINO3.4 index running variance ($^{\circ}\text{C}^2$) in 30-year sliding window for all models for LM simulations. Variance is shown as the normalised anomaly (variance is divided by its standard deviation for each model) to assist with comparison between models. The multi-model (MM) mean is also shown (*thick black line*). The dates of major volcanic eruptions at 1258, 1452 and 1815 are shown as *vertical dashed lines* for reference



comparison between models (Fig. 7). Unlike the regional temperature record (Fig. 5a), there are no common multi-decadal periods of high or low ENSO variance for all models. The multi-model mean (thick black line in Fig. 7) indicates significantly increased variance around 1250 and after 1800 (the anomaly is designated significant if the 10-year mean is above the 95th percentile of values calculated from running 10-year blocks of the record), but all models do not agree on the sign of the anomaly.

Previous studies using proxy-based reconstructions have identified modulations of ENSO variance on decadal and longer timescales. For example, McGregor et al. (2010) found low variance from around 1650–1720, while Li et al. (2011) and Li et al. (2013) found low ENSO variance at the beginning of the Little Ice Age, around 1300–1550, and increased variance in the period 1550–1880. The lack of coherent periods of high and low variance between the six CMIP5–PMIP3 models suggests that the variability is not externally forced. This is consistent with a previous Monte-Carlo analysis showing the range of reconstructed ENSO variance prior to 1900 may arise stochastically (Li et al. 2013). The conclusion that ENSO variability over the last millennium was primarily driven by internal dynamics was also reached in other proxy-based studies (e.g. McGregor et al. 2010), and model studies (Landrum et al. 2013).

4.3 Variability of ENSO–rainfall teleconnections

We have identified temporal variability in the strength of the relationship between ENSO and Australian rainfall in the historical climate (Sect. 3). Variability of ENSO–rainfall teleconnections in past climate has also been identified in previous studies (e.g. McGregor et al. 2013). In particular, Gallant et al. (2013) identified non-stationarity of teleconnections between ENSO and Australian rainfall in instrumental records, model simulations and palaeoclimate reconstructions on near-centennial timescales. We therefore

investigate the temporal and spatial variability of the relationship between ENSO and eastern Australian rainfall in the CMIP5–PMIP3 LM simulations.

The temporal variability of the strength of the ENSO–eastern Australian rainfall teleconnection in the LM simulations was examined using the 30-year running correlation between SONDJF eastern Australian rainfall and NINO3.4 index (Fig. 8). The running variance of ENSO is also shown in Fig. 8 for comparison, to determine whether changes in teleconnection strength follow changes in ENSO strength. All models simulate variation in the strength of the ENSO–eastern Australian rainfall teleconnection in the LM simulations, including periods of near-zero or even positive correlations. Such variations would potentially reduce the ability of palaeoclimate proxy records from eastern Australia to capture information about ENSO behaviour, at least during periods of weakened teleconnection, in agreement with Gallant et al. (2013).

In all cases, the ENSO–eastern Australian rainfall correlation is significantly inversely correlated with ENSO variance (correlation coefficients are given in Fig. 8, $p < 0.01$ in all cases). This is consistent with the relationships identified in the HIST simulations (Fig. 4). Our results are also in qualitative agreement with Li et al. (2013), who found that ENSO teleconnections over the Pacific region in a range of proxy records for the past seven centuries were strong when ENSO variance was high and weak when ENSO variance was low. In most cases, correlations between ENSO variance and the strength of the ENSO–rainfall running correlation are substantially weaker for the LM simulations than for the HIST simulations (Fig. 4), with the exception of CCSM4 and CSIRO-Mk3L models, which have a low correlation in both simulations. The relatively weak correlations between ENSO variance and ENSO–rainfall teleconnection strength in the LM simulations indicate that internal variability is responsible for most of the variation in teleconnection strength.

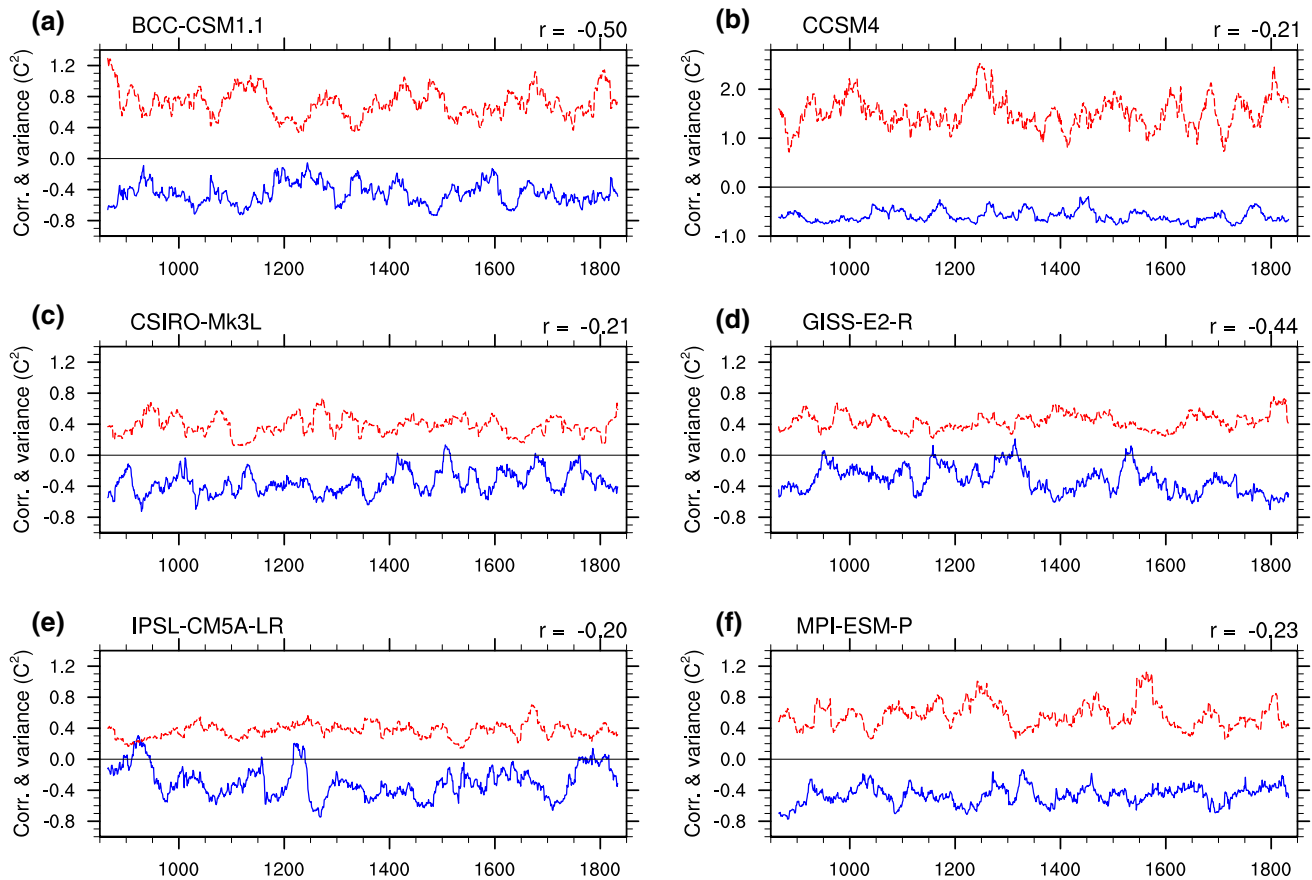


Fig. 8 30-year running correlations of September to February eastern Australian rainfall and NINO3.4 index (blue solid line) and 30-year running variance ($^{\circ}\text{C}^2$) of SONDJF NINO3.4 index (red dashed line) for LM simulations (850–1850). All time series were lin-

early detrended before calculating running correlations. Correlations between the two time series are given at the top right. Note (b) has different y-axis scale

The stability of the spatial pattern of the ENSO–rainfall teleconnection in the Australian region was also examined. Firstly, the 1000-year average spatial correlation between NINO3.4 and SONDJF rainfall was calculated for the LM simulations (Supplementary Figure 2). The long-term average LM spatial patterns are largely unchanged from the HIST simulations (Fig. 2), with pattern correlations between HIST and LM spatial patterns of $r > 0.9$ in all cases. This implies that the mean large-scale teleconnection pattern is stable over the LM simulations, and also that there is no strong anthropogenic influence on the average teleconnection pattern for the HIST simulations.

Despite the stability of the long-term average teleconnection patterns, there may be non-stationarity of the teleconnection pattern on decadal and longer time scales within the LM simulations. We investigate teleconnection stationarity by comparing the spatial correlation pattern in the HIST simulations with the spatial correlation pattern calculated for 30-year segments of the LM simulations for each model. A similar approach was applied by Coats et al. (2013) in a study of ENSO teleconnections over North

America. The temporal correlation between NINO3.4 and SONDJF rainfall at each grid point was calculated for moving 30-year windows of the LM simulation from 850 to 1850. The running pattern correlation (“R_PC”) between the average HIST and time-varying LM spatial teleconnection patterns was then calculated (in the domain 15°N – 50°S , 100°E – 160°W), and the resulting time series of correlation coefficients are shown in Fig. 9.

The average running pattern correlation coefficients between model HIST and LM NINO3.4–rainfall correlation patterns range from $R_{\text{PC}} = 0.92$ (CCSM4) to $R_{\text{PC}} = 0.81$ (CSIRO-Mk3L), with periods of reduced correlation strength occurring for all models, implying non-stationarity of the ENSO–rainfall teleconnection over the Australian region. The extent of teleconnection non-stationarity can be measured from the standard deviation of R_{PC} , which is greatest for CSIRO-Mk3L and IPSL-CM5A-R and smallest for CCSM4 (see Fig. 9). In a study of teleconnection stationarity over North America using CMIP5–PMIP3 models, Coats et al. (2013) found non-stationarity was smaller in models with larger ENSO

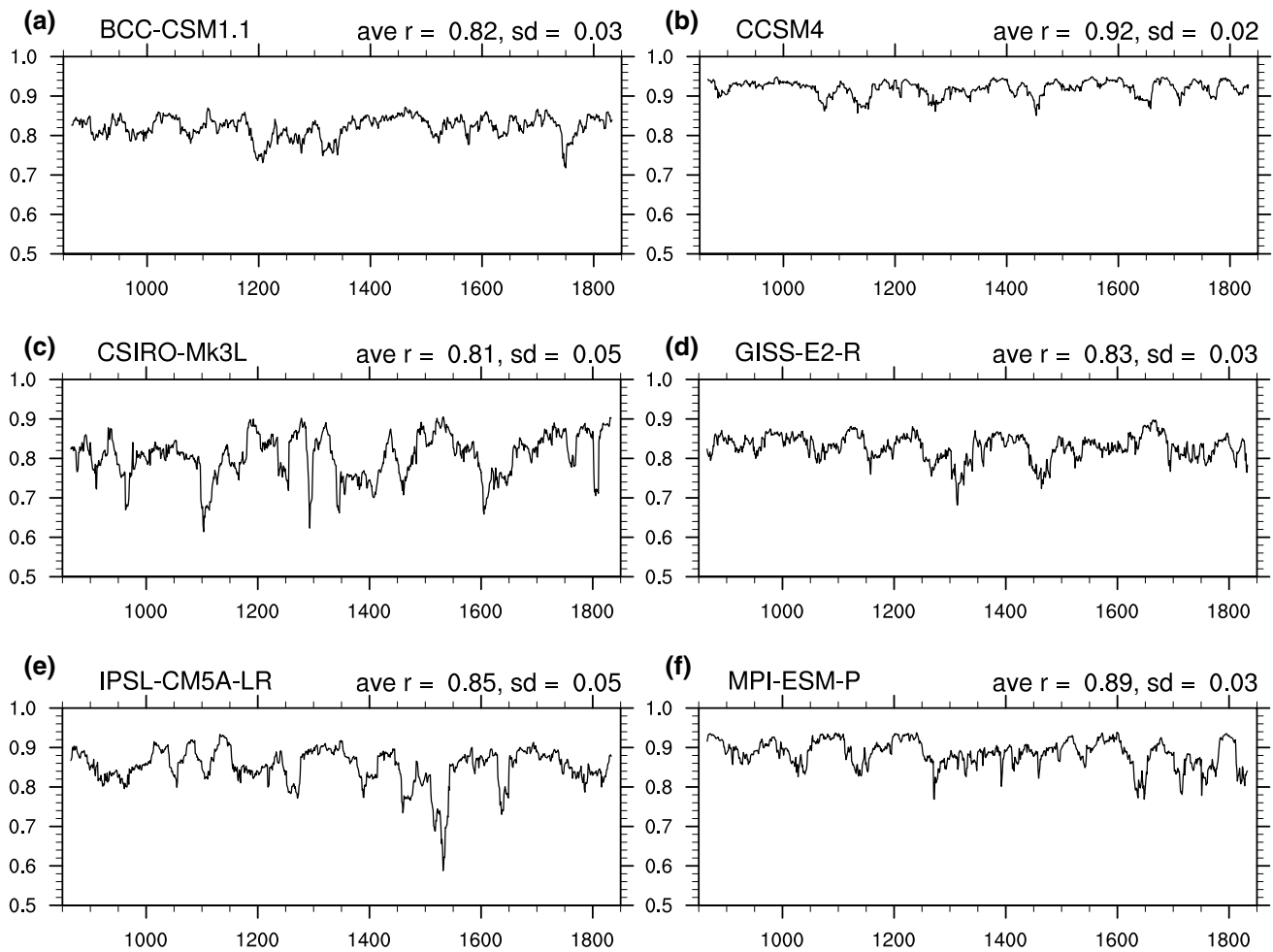


Fig. 9 Running spatial pattern correlation (R_{PC}) between SONDJF NINO3.4-rainfall correlation pattern for HIST simulations and SONDJF NINO3.4-rainfall correlation pattern for 30-year segments of LM simulations. Model HIST correlation patterns are

shown in Fig. 2. Spatial correlations are calculated over the domain 15°N – 50°S , 100°E – 160°W . The average and standard deviation of R_{PC} for each model is given at *top right*

amplitude. In this study, we also find that the model with the largest ENSO amplitude (CCSM4) displays the smallest non-stationarity (smallest R_{PC} standard deviation) of teleconnections in the Australian region, while the models with greater teleconnection non-stationarity had a smaller ENSO amplitude (CSIRO-Mk3L and IPSL-CM5A-R).

In the CMIP5–PMIP3 LM simulations, we find that variability occurred in both the strength of the ENSO–eastern Australian rainfall teleconnection and the spatial pattern of the ENSO–rainfall teleconnection over the wider Australian region. While the running temporal correlation of ENSO with eastern Australian rainfall weakens to near-zero values for multi-decadal periods in all models (Fig. 8), the regional spatial teleconnection pattern is more robust, with the running pattern correlation (R_{PC}) between HIST and LM ENSO–rainfall teleconnection patterns remaining in the range 0.7–0.9 throughout the 1000 year simulations

in most cases (Fig. 9). This result is in agreement with McGregor et al. (2013), who found that ENSO variance and rainfall variance in the Pacific region could have zero or even negative correlations at particular locations, whereas comparison of multiple locations produced a more robust relationship between ENSO variability and rainfall variability.

5 Discussion and conclusions

The variability of eastern Australian rainfall was examined in simulations of the historical period and the last millennium (850–1850) from a set of six CMIP5–PMIP3 coupled climate models. The ability of the models to capture the main characteristics of modern ENSO and Australian-region rainfall teleconnections was variable, with the

IPSL-CM5A-LR model simulating low rainfall variability and a poor ENSO teleconnection. The BCC-CSM1-1 and GISS-E2-R models also failed to capture aspects of the observed ENSO and rainfall climatology, while the CSIRO-Mk3L model had an overly weak correlation between eastern Australian rainfall and ENSO. CCSM4 had an overly strong ENSO variance, while MPI-ESM-P had the most plausible simulation of the modern eastern Australian rainfall–ENSO relationship. However, we utilise all six models in recognition that the observed ENSO characteristics of the instrumental period may not capture all plausible states of ENSO.

In the last millennium simulations, the models simulated some common features of regional eastern Australian temperature, including decadal-scale cooling following major volcanic eruptions and a long-term cooling trend. An increase in eastern Australian rainfall was also simulated by the majority of models during the period following the major volcanic eruptions, with a significant anomaly in the multi-model mean. However, the lack of significant correlations between model eastern Australian rainfall indicates that rainfall variability in this region is primarily driven by internal processes in each climate model, including ENSO, rather than by external forcing.

The NINO3.4 SST anomaly in the LM simulations also displays common cooling associated with major volcanic events in all models. The signal is also seen in the corresponding equatorial Southern Oscillation Index (an atmospheric pressure index of ENSO), so does not simply reflect regional SST cooling but also a reorganisation of the climate in an ENSO-like manner (e.g. Adams et al. 2003; Mann et al. 2005; Emile-Geay et al. 2008). Further examination of the response to volcanic forcing is beyond the scope of this study, but we note that our results are consistent with other studies examining CMIP5–PMIP3 last millennium simulations, which found a strong model response to volcanic forcing in the NINO3.4 region on decadal to centennial timescales (Ault et al. 2013; Landrum et al. 2013). In addition, the NINO3.4 index displays variability on decadal and longer time scales that differs between models, suggesting a large role for internal variability. This is consistent with other studies (e.g. Wittenberg 2009; Wittenberg et al. 2014) that report large internal variability of ENSO in long unforced control simulations. Note, however, that models may still underestimate the natural decadal to multi-decadal variability of ENSO (Emile-Geay et al. 2013) and of rainfall (Ault et al. 2012).

The teleconnection between ENSO and eastern Australian rainfall varies in strength in all models in the LM simulations, in a similar manner to the variability found in the HIST simulations. Periods of very weak running correlation occur in all models, indicating temporary breakdowns

in the ENSO–eastern Australian rainfall relationship. Interestingly, these do not appear to be associated with periods of reduced ENSO variance in most cases, although all models simulate a significant negative correlation between ENSO variance and running ENSO–rainfall correlation (teleconnection) strength. The large-scale climate state during these periods of teleconnection breakdown was investigated using composites (not shown), but no consistent change in mean state was identified. Instead, we suggest that periods of weak eastern Australian rainfall–ENSO teleconnection may reflect a range of other influences on eastern Australian rainfall, both tropical and high latitude, on a range of time scales (e.g. Risbey et al. 2009). Further analysis is required to investigate these influences in more detail.

The regional spatial pattern of the ENSO–rainfall teleconnection was found to be stable on average over the LM simulations, with close agreement between the long-term average LM and HIST patterns. However, there was some variability of the teleconnection spatial pattern on decadal timescales, indicated by variation in the running pattern correlation for 30-year segments of the LM simulations. If this variability is correctly represented by the models, then it implies that non-stationarity of ENSO–rainfall teleconnections may present challenges for quantitative reconstruction of ENSO behaviour using rainfall-sensitive proxy records from the Australian region.

In conclusion, the relationship between eastern Australian rainfall and ENSO is found to be non-stationary in a set of six climate model simulations of the last millennium, in agreement with previous studies (e.g. Hendy et al. 2003; Gergis et al. 2012; Gallant et al. 2013). The time-variability of the teleconnection strength is greater than the time-variability of the teleconnection spatial pattern, in agreement with other studies (e.g. McGregor et al. 2013). Comparison of the CMIP5–PMIP3 model results with proxy reconstructions of Australian rainfall and ENSO over the last millennium would provide further insights into the non-stationarity of the ENSO–rainfall teleconnection.

Acknowledgments The contribution of JRB and PH was supported by the Australian Climate Change Science Program. JG is supported by an Australian Research Council Fellowship DE130100668. BH is funded by an ARC Cooperative Research Network (CRN) research grant. We acknowledge the World Climate Research Programme's Working Group on Coupled Modelling, which is responsible for CMIP, and we thank the climate modelling groups for producing and making available their model output. For CMIP the U.S. Department of Energy's Program for Climate Model Diagnosis and Intercomparison provides coordinating support and led development of software infrastructure in partnership with the Global Organization for Earth System Science Portals. We thank Greg Kociuba for calculation of the equatorial SOI. We thank an anonymous reviewer for comments that greatly improved the manuscript. We also thank Sophie Lewis for discussion of model evaluation, and Ian Smith and Christine Chung for comments on an earlier version of the manuscript.

References

- Adams J, Mann M, Ammann C (2003) Proxy evidence for an El Niño-like response to volcanic forcing. *Nature* 426:274–278. doi:[10.1038/nature02101](https://doi.org/10.1038/nature02101)
- Adler RF et al (2003) The version 2 global precipitation climatology project (GPCP) monthly precipitation analysis (1979–present). *J Hydrometeorology* 4:1147–1167
- Arblaster J, Meehl G, Moore A (2002) Interdecadal modulation of Australian rainfall. *Clim Dyn* 18:519–531
- Ashcroft L, Karoly DJ, Gergis J (2014) Southeastern Australian climate variability 1860–2009: a multivariate analysis. *Int J Climatol* 34:1928–1944. doi:[10.1002/joc.3812](https://doi.org/10.1002/joc.3812)
- Ault TR, Cole JE, St. George S (2012) The amplitude of decadal to multidecadal variability in precipitation simulated by state-of-the-art climate models. *Geophys Res Lett* 39:L21705. doi:[10.1029/2012GL053424](https://doi.org/10.1029/2012GL053424)
- Ault TR, Deser C, Newman M, Emile-Geay J (2013) Characterizing decadal to centennial variability in the equatorial Pacific during the last millennium. *Geophys Res Lett* 40:3450–3456. doi:[10.1002/grl.50647](https://doi.org/10.1002/grl.50647)
- Braconnot P, Harrison SP, Kageyama M, Bartlein PJ, Masson-Delmotte V, Abe-Ouchi A, Otto-Bliesner B, Zhao Y (2012) Evaluation of climate models using palaeoclimatic data. *Nat Clim Change* 2:417–424. doi:[10.1038/NCLIMATE1456](https://doi.org/10.1038/NCLIMATE1456)
- Bretherton CS, Widmann M, Dymnikov VP, Wallace JM, Bladé I (1999) The effective number of spatial degrees of freedom of a time-varying field. *J Clim* 12:1990–2009
- Brown JR, Moise AF, Colman RA (2013) The South Pacific Convergence Zone in CMIP5 simulations of historical and future climate. *Clim Dyn* 41:2179–2197. doi:[10.1007/s00382-012-1591-x](https://doi.org/10.1007/s00382-012-1591-x)
- Cai W, van Rensch P (2012) The 2011 southeast Queensland extreme summer rainfall: a confirmation of a negative Pacific Decadal Oscillation phase? *Geophys Res Lett* 39:L08702. doi:[10.1029/2011GL050820](https://doi.org/10.1029/2011GL050820)
- Coats S, Smerdon JE, Cook BI, Seager R (2013) Stationarity of the tropical Pacific connection to North America in CMIP5/PMIP3 model simulations. *Geophys Res Lett* 40:4927–4932. doi:[10.1002/grl.50938](https://doi.org/10.1002/grl.50938)
- Diaz HF, Hoerling MP, Eischeid JK (2001) ENSO variability, teleconnections and climate change. *Int J Climatol* 21:1845–1862. doi:[10.1002/joc.631](https://doi.org/10.1002/joc.631)
- Emile-Geay J, Seager R, Cane M, Cook E, Haug GH (2008) Volcanoes and ENSO over the past millennium. *J Clim* 21:3134–3148. doi:[10.1175/2007JCLI11884.1](https://doi.org/10.1175/2007JCLI11884.1)
- Emile-Geay J, Cobb KM, Mann ME, Wittenberg AT (2013) Estimating central equatorial Pacific SST variability over the past millennium. Part II: reconstruction and implications. *J Clim* 26:2329–2352. doi:[10.1175/JCLI-D-11-00511.1](https://doi.org/10.1175/JCLI-D-11-00511.1)
- Fernández-Donado L et al (2013) Large-scale temperature response to external forcing in simulations and reconstructions of the last millennium. *Clim Past* 9:393–421. doi:[10.5194/cp-9-393-2013](https://doi.org/10.5194/cp-9-393-2013)
- Gallant A, Kiem A, Verdon-Kidd D, Stone R, Karoly D (2012) Understanding climate processes in the Murray-Darling basin for natural resources management. *Hydrol Earth Syst Sci* 16:2049–2068
- Gallant AJE, Phipps SJ, Karoly DJ, Mullan AB, Lorrey AM (2013) Non-stationary Australasian teleconnections and implications for paleoclimate reconstructions. *J Clim* 26:8827–8849. doi:[10.1175/JCLI-D-12-00338.1](https://doi.org/10.1175/JCLI-D-12-00338.1)
- Gergis J, Gallant AJE, Braganza KA, Karoly DJ, Allen K, Cullen L, D'Arrigo R, Goodwin I, Grierson P, McGregor S (2012) On the long-term context of the 1997–2009 'Big Dry' in south-eastern Australia: insights from a 206-year multi-proxy rainfall reconstruction. *Clim Change* 111:923–944. doi:[10.1007/s10584-011-0263-x](https://doi.org/10.1007/s10584-011-0263-x)
- Grose MR, Brown JN, Narsey S, Brown JR, Murphy BF, Langlais C, Sen Gupta A, Moise AF, Irving DB (2014) Assessment of the CMIP5 global climate model simulations of the western tropical Pacific climate system and comparison to CMIP3. *Int J Climatol* 34:3382–3399. doi:[10.1002/joc.3916](https://doi.org/10.1002/joc.3916)
- Hendy E, Gagan M, Lough J (2003) Chronological control of coral records using luminescent lines and evidence for non-stationary ENSO teleconnections in northeastern Australia. *The Holocene* 13:187–199
- Jones DA, Wang W, Fawcett R (2009) High-quality spatial climate data-sets for Australia. *Aust Meteorol Oceanogr* J 58:233–248
- Kestin T, Karoly D, Yano JI (1998) Time–frequency variability of ENSO and stochastic simulations. *J Clim* 11:2258–2272
- King AD, Donat MG, Alexander LV, Karoly DJ (2014) The ENSO–Australian rainfall teleconnection in reanalysis and CMIP5. *Clim Dyn*. doi:[10.1007/s00382-014-2159-8](https://doi.org/10.1007/s00382-014-2159-8)
- Landrum L, Otto-Bliesner BL, Wahl ER, Conley A, Lawrence PJ, Rosenbloom N, Teng H (2013) Last millennium climate and its variability in CCSM4. *J Clim* 26:1085–1111. doi:[10.1175/JCLI-D-11-00326.1](https://doi.org/10.1175/JCLI-D-11-00326.1)
- Lewis SC, Karoly DJ (2015) Are estimates of anthropogenic and natural influences on Australia's extreme 2010–2012 rainfall model-dependent? *Clim Dyn* 45:679–695. doi:[10.1007/s00382-014-2283-5](https://doi.org/10.1007/s00382-014-2283-5)
- Li J, Xie S-P, Cook ER, Huang G, D'Arrigo R, Liu F, Ma J, Zheng X-T (2011) Interdecadal modulation of El Niño amplitude during the past millennium. *Nat Clim Change* 1:114–118. doi:[10.1038/NCLIMATE1086](https://doi.org/10.1038/NCLIMATE1086)
- Li J et al (2013) El Niño modulations over the past seven centuries. *Nat Clim Change* 3:822–826. doi:[10.1038/NCLIMATE1936](https://doi.org/10.1038/NCLIMATE1936)
- Mann ME, Cane MA, Zebiak SE, Clement A (2005) Volcanic and solar forcing of the tropical Pacific over the past 1000 years. *J Clim* 18:447–456
- Masson-Delmotte V, Schulz M, Abe-Ouchi A, Beer J, Ganopolski A, González Rouco JF, Jansen E, Lambeck K, Luterbacher J, Naish T, Osborn T, Otto-Bliesner B, Quinn T, Ramesh R, Rojas M, Shao X, Timmermann A (2013) Information from paleoclimate archives. In: Stocker TF, Qin D, Plattner G-K, Tignor M, Allen SK, Boschung J, Nauels A, Xia Y, Bex V, Midgley PM (eds) *Climate change 2013: the physical science basis*. Contribution of Working Group I to the Fifth Assessment Report of the Intergovernmental Panel on Climate Change. Cambridge University Press, Cambridge
- McGregor S, Timmermann A (2011) The effect of explosive tropical volcanism on ENSO. *J Clim* 24:2178–2191. doi:[10.1175/2010JCLI3990.1](https://doi.org/10.1175/2010JCLI3990.1)
- McGregor S, Timmermann A, Timm O (2010) A unified proxy for ENSO and PDO variability since 1650. *Clim Past* 6:1–17. doi:[10.5194/cp-6-1-2010](https://doi.org/10.5194/cp-6-1-2010)
- McGregor S, Timmermann A, England MH, Timm OE, Wittenberg AT (2013) Inferred changes in El Niño–Southern Oscillation variance over the past six centuries. *Clim Past* 9:2269–2284. doi:[10.5194/cp-9-2269-2013](https://doi.org/10.5194/cp-9-2269-2013)
- Neukom R, Gergis J (2012) Southern Hemisphere high-resolution palaeoclimate records of the last 2000 years. *The Holocene* 22:501–524. doi:[10.1177/0959683611427335](https://doi.org/10.1177/0959683611427335)
- Nicholls N, Drosowsky W, Lavery B (1997) Australian rainfall variability and change. *Weather* 52:66–71
- PAGES 2 k Consortium (2013) Continental-scale temperature variability during the past two millennia. *Nat Geosci* 6:339–346. doi:[10.1038/ngeo1797](https://doi.org/10.1038/ngeo1797)
- Power SB, Kociuba G (2011) The impact of global warming on the Southern Oscillation Index. *Clim Dyn* 37:1745–1754. doi:[10.1007/s00382-010-0951-7](https://doi.org/10.1007/s00382-010-0951-7)
- Power S, Tseitkin F, Torok S, Lavery B, Dahni R, McAvaney B (1998) Australian temperature, Australian rainfall and the Southern

- Oscillation, 1910–1992: coherent variability and recent changes. *Aust Meteorol Mag* 47:85–101
- Power S, Casey T, Folland C, Colman A, Mehta V (1999) Inter-decadal modulation of the impact of ENSO on Australia. *Clim Dyn* 15:319–324
- Power S, Haylock M, Colman R, Wang X (2006) The predictability of interdecadal changes in ENSO activity and ENSO teleconnections. *J Clim* 19:4755–4771
- Rasmusson E, Carpenter T (1982) Variations in tropical sea surface temperature and surface wind fields associated with the Southern Oscillation/El Niño. *Mon Weather Rev* 110:354–384
- Risbey JS, Pook MJ, McIntosh PC, Wheeler MC, Hendon HH (2009) On the remote drivers of rainfall variability in Australia. *Mon Weather Rev* 137:3233–3253
- Ropelewski CF, Halpert MS (1987) Global and regional scale precipitation patterns associated with the El Niño/Southern Oscillation. *Mon Weather Rev* 115:1606–1626
- Schmidt GA, Jungclaus JH, Ammann CM, Bard E, Braconnot P, Crowley TJ, Delaygue G, Joos F, Krivova NA, Muscheler R, Otto-Bliesner BL, Pongratz J, Shindell DT, Solanki SK, Steinhilber F, Vieira LE (2012) Climate forcing reconstructions for use in PMIP simulations of the last millennium (v1.1). *Geosci Model Dev* 5:185–191. doi:[10.5194/gmd-5-185-2012](https://doi.org/10.5194/gmd-5-185-2012)
- Schmidt GA, Annan JD, Bartlein PJ, Cook BI, Guilyardi E, Hargreaves JC, Harrison SP, Kageyama M, LeGrande AN, Konecky B, Lovejoy S, Mann ME, Masson-Delmotte V, Risi C, Thompson D, Timmermann A, Tremblay LB, Yiou P (2014) Using palaeoclimate comparisons to constrain future projections in CMIP5. *Clim Past* 10(1):221–250. doi:[10.5194/cp-10-221-2014](https://doi.org/10.5194/cp-10-221-2014)
- Smith TM, Reynolds RW (2004) Improved extended reconstruction of SST (1854–1997). *J Clim* 17:2466–2477
- Taylor KE, Stouffer RJ, Meehl GA (2012) An overview of CMIP5 and the experiment design. *Bull Am Meteorol Soc* 93:485–498. doi:[10.1175/BAMS-D-11-00094.1](https://doi.org/10.1175/BAMS-D-11-00094.1)
- Vincent EM, Lengaigne M, Menkes CE, Jourdain NC, Marchesiello P, Madec G (2011) Interannual variability of the South Pacific Convergence Zone and implications for tropical cyclone genesis. *Clim Dyn* 36:1881–1896. doi:[10.1007/s00382-009-0716-3](https://doi.org/10.1007/s00382-009-0716-3)
- Wang G, Hendon H (2007) Sensitivity of Australian rainfall to inter-El Niño variations. *J Clim* 20:4211–4226. doi:[10.1175/JCLI4228.1](https://doi.org/10.1175/JCLI4228.1)
- Wittenberg AT (2009) Are historical records sufficient to constrain ENSO simulations? *Geophys Res Lett* 36:L12702. doi:[10.1029/2009GL038710](https://doi.org/10.1029/2009GL038710)
- Wittenberg AT, Rosati A, Delworth TL, Vecchi GA, Zeng F (2014) ENSO modulation: is it decadal predictable? *J Clim* 27:2667–2681. doi:[10.1175/JCLI-D-13-00577.1](https://doi.org/10.1175/JCLI-D-13-00577.1)